Aydemir, T., Şahin, M. (2024). Kurtosis Rejection-Based Person Identification from Photoplethysmography Signals Recorded During a Step Exercise. *The Black Sea Journal of Sciences*, 14(4), 1825-1835.

The Black Sea Journal of Sciences, 14(4), 1825-1835, 2024. DOI: 10.31466/kfbd.1492325

KFBD

Karadeniz Fen Bilimleri Dergisi
The Black Sea Journal of Sciences
ISSN (Online): 2564-7377 https://dergipark.org.tr/tr/pub/kfbd

Araştırma Makalesi / Research Article

Kurtosis Rejection-Based Person Identification from Photoplethysmography Signals Recorded During a Step Exercise

Tuğba AYDEMİR[1*], Mehmet ŞAHİN[2]

Abstract

In addition to computer vision-based methods, physiological signal-based person identification (PI) applications have attracted great attention in recent years with various kinds of advantages. Because physical activities can significantly contaminate physiological signals, most of the PI models were proposed to acquire the considered signal during the resting state. In this study, we proposed a kurtosis rejection-based PI from photoplethysmography (PPG) signals recorded during a step exercise. In the preprocessing stage, we rejected the PPG trials, which have a kurtosis value greater than five and are labeled as non-PPG, from the classification process. Afterward, the features were extracted by the sequential forward mother wavelet selection method and classified using the *k*-nearest neighbor algorithm. We achieved the highest classification accuracy rate of 88.64% PI performance. The obtained results proved that the kurtosis rejection-based PPG signals recorded during the step exercise can be reliably used for PI.

Keywords: Person identification, Kurtosis, Photoplethysmography, Wavelet selection, Sequential forward, Feature extraction, Classification.

Adım Egzersizi Sırasında Kaydedilen Fotopletismografi Sinyallerinden Basıklık Reddine Dayalı Kişi Tanımlaması

Öz

Bilgisayarlı görü tabanlı yöntemlerin yanı sıra, fizyolojik sinyal tabanlı kişi tanımlama (KT) uygulamaları da çeşitli avantajlarıyla son yıllarda büyük ilgi görmektedir. Fiziksel aktiviteler fizyolojik sinyalleri önemli ölçüde kirletebildiğinden, KT modellerinin çoğu, dikkate alınan sinyali dinlenme durumu sırasında elde etmek için önerilmiştir. Bu çalışmada, bir adım egzersizi sırasında kaydedilen fotopletismografi (PPG) sinyallerinden basıklık reddine dayalı bir KT önerilmiştir. Ön işleme aşamasında basıklık değeri beşten büyük olan ve PPG olmayan olarak etiketlenen PPG denemelerini sınıflandırma sürecinden çıkarılmıştır. Daha sonra sıralı ileri ana dalgacık seçim yöntemiyle öznitelikler çıkarılmış ve k-en yakın komşu algoritması kullanılarak sınıflandırılmıştır. %88.64 KT performansıyla en yüksek sınıflandırma doğruluğu oranına ulaşılmıştır. Elde edilen sonuçlar, adım egzersizi sırasında kaydedilen basıklık reddine dayalı PPG sinyallerinin KT için güvenilir bir şekilde kullanılabileceğini doğrulamıştır.

Anahtar Kelimeler: Kişi tanımlama, Basıklık, Fotopletismografi, Dalgacık seçimi, Sıralı ileri, Özellik çıkarımı, Sınıflandırma.

[1]Recep Tayyip Erdogan University, Department of Physics, Rize, Türkiye, tugba_aydemir17@erdogan.edu.tr mehmet.sahin@erdogan.edu.tr

[*]Sorumlu Yazar/Corresponding Author
Geliş/Received: 30.05.2024 **Kabul/Accepted:** 30.09.2024 **Yayın/Published:** 15.12.2024

1. Introduction

Person identification (PI) is the process of recognizing a person from a group by comparing newly extracted features to their corresponding baseline values, extracted from signals recorded earlier. Computer vision-based PI studies have mostly been reported (Bedagkar-Gala and Shah, 2014; Chao et al., 2020; Kim et al., 2021) because as public security and safety demands increase every day, biometric PI-based studies have attracted significant interest in recent years (Jijomon and Vinod, 2021; Mazaira-Fernandez et al., 2015; Aydemir, 2020). The biometric PI uses physiological and/or behavioral characteristics of a person, such as voice, fingerprint, signature, retina, iris, electroencephalography, and near-infrared spectroscopy. Each technique has a proper and limited application field and its pros and cons. For example, fingerprints might be dirty, cut, or tear and can be reproduced using a latex or gummy finger, face identification can be fraudulent by a photo, a person might be wearing glasses or eye lenses for iris identification, and voice can be synthesized or pre-recorded. Therefore, newly developed biometric PI-based methods have been yet proposed.

Developments in biosensor technology help realize new or high-performance applications including monitoring individual health metrics, allowing usage of wireless brain-computer interfaces, and admitting alternative biometric PI systems. It can be said that these advances offer to establish robust and accurate human identification systems, which are difficult to be stolen or hacked, and proof of liveness since they only exist if the person is alive. Physiological signals like electroencephalography (Rodrigues et al., 2016; Alyasseri et al., 2020; Wilaiprasitporn et al., 2019), electromyography (Li et al., 2020a; Lu et al., 2020; He and Jiang, 2020), and electrocardiography (Pinto et al., 2017; Li et al., 2020b; Wu et al., 2018) have also been used for PI approaches. Due to such kinds of systems requiring many electrodes attached to different parts of the body to acquire signals, they might not be practical for real-life biometric applications (Siam et al., 2021). Compared with other physiological signals, photoplethysmography (PPG) has received considerable attention for PI approaches in the last few years since it is a non-invasive, easily acquired, portable, and low-cost technique that takes measures from the skin surface.

In a PPG-based human identification study, Siam et al. used a dataset of PPG signals recorded from 35 healthy persons (50 to 60 6-seconds-PPG trials for each one). The features were extracted by the Mel frequency cepstral coefficients, which fed into an artificial neural network classifier. Although they achieved 100% classification accuracy (CA) rate using the holdout cross-validation method, an unseen test set CA rate was not reported (Siam et al., 2021). In another study, Kavsaoglu et al. proposed a feature ranking algorithm for biometric recognition with PPG signals, where each trial included 15 periods

(Kavsaoğlu et al., 2014). They obtained the dataset from 30 subjects, who were seated in a calm position. They reached a maximum CA rate of 94.44% by using time-domain features of the first and second derivatives of the PPG signals. In another PPG-based biometric study, Xiao et al. achieved a CA rate of 91.31% by using wavelet transform features (Xiao et al., 2019). They recorded the dataset from 23 subjects who were in a relaxed position. To the best of our knowledge, instead of the signals recorded in the relaxed position of the subjects in the literature, this study was the first work attempting to identify a person from PPG signals during recorded stepper activity. In this way, it has been shown that PPG signals can be used in person recognition not only in a relaxed state but also when people are recorded while they are moving. Because the stepper exercise might contaminate the PPG signals at an unanalyzable level, we proposed a kurtosis rejection-based person identification method to increase the CA performance. It is also worth mentioning that we tested 3-s, 4-s, 5-s, 6-s, and 7-s length PPG trials with thirteen wavelets. The proposed method was successfully applied to the same dataset and achieved a CA rate of 88.64%.

After the introduction section, the rest of the paper is organized as follows. In section 2, first, the dataset and preprocessing description are given. Afterward, the feature extraction techniques and sequential forward mother wavelet selection (SFMWS) method are introduced in detail. In section 3, the results are given in tables. Finally, we concluded the results in the last section and discussed the findings.

2. Material and Methods

In the following subsections, first, the dataset used is described. Afterward, the parts of the proposed method are introduced in detail.

2.1. Data Set and Preprocessing Description

In this study, the PPG signals were recorded from three males and four females aged between 20 and 52 years during a voluntary step exercise (Aydemir et al., 2020; Biagetti et al., 2020). The signals were acquired with a sampling frequency of 400 Hz using the wrist using the wireless Maxim Integrated MAXREFDES100 equipment. A specific and elastic weightlifting cuff has been used to have better signal quality and ensure a tight junction between the skin surface and the PPG sensor. It had an adjustable property by a tear-off closure. After all participants gave informed written consent, they performed five acquisition sessions. Table 1 shows the total acquisition time for each subject (S1, S2,…, S7). The proposed kurtosis rejection-based method was applied by splitting the PPG signals into the 3 s,

4 s, 5 s, 6 s, and 7 s segments (trials). It is worthwhile to mention that because the data splitting process was done session by session, the total number of trials might not be equal to the total acquisition time.

Table 1. Total recording time and number of trials

		S1	S2	S3	S4	S5	S6	S7
Whole dataset	Total time (second)	443.0	397.6	271.0	269.7	242.0	325.9	254.9
Number of trials for 3 s	Before elimination	146	130	88	87	78	107	83
	After elimination	115	99	71	66	63	93	65
Number of trials for 4 s	Before elimination	110	111	111	111	57	79	61
	After elimination	85	86	92	86	48	67	45
Number of trials for 5 s	Before elimination	86	76	52	51	47	63	49
	After elimination	78	63	50	45	43	61	43
Number of trials for 6 s	Before elimination	72	73	43	43	37	53	41
	After elimination	63	57	35	36	28	46	30
Number of trials for 7 s	Before elimination	61	54	36	36	32	44	34
	After elimination	57	49	35	32	27	44	30

After close observation of the signals, we realized that some segments were substantially contaminated by physical activity noise and did not show the properties of a PPG signal. For this reason, we utilized a kurtosis-based threshold level to omit such kinds of trials (non-PPG trials) from the classification dataset. The kurtosis value was calculated as follows

$$Kurtosis = \frac{\frac{1}{L}\sum_{i=1}^{L}(x_i - \bar{x})}{\left(\frac{1}{L}\sum_{i=1}^{L}(x_{i-}\bar{x})^2\right)^2} \quad (1)$$

where x_i is the i^{th} sample of a trial x, $\bar{x}$ is the mean value of x, and L is the length of a trial. Some examples of such 3-s trials are shown in Figure 1. We empirically decided the kurtosis threshold level as five, where any PPG trial has a kurtosis value bigger than five, we rejected this trial from feature extraction and classification procedures. This value was found empirically. While the first line of this figure shows 3-s length PPG trials, which have a kurtosis value smaller than five, the second line illustrates PPG trials, with a kurtosis value bigger than five. In order to decide on the non-PPG trial, we used kurtosis because it was a measure of the combined size of two tails. Additionally, it is often used as a quantitative measure of the non-Gaussianity of a random signal. Therefore, it can be used as a simple

measure of PPG and non-PPG (Choi and Lee, 2021; Zhang and Ding, 2016). After that process, the number of considered trials is also given in Table 1. The main purpose is to classify the trials in the test set as S1, S2,…, S7. Note that we randomly selected half of the trials as the training set and the rest of them as the test set.

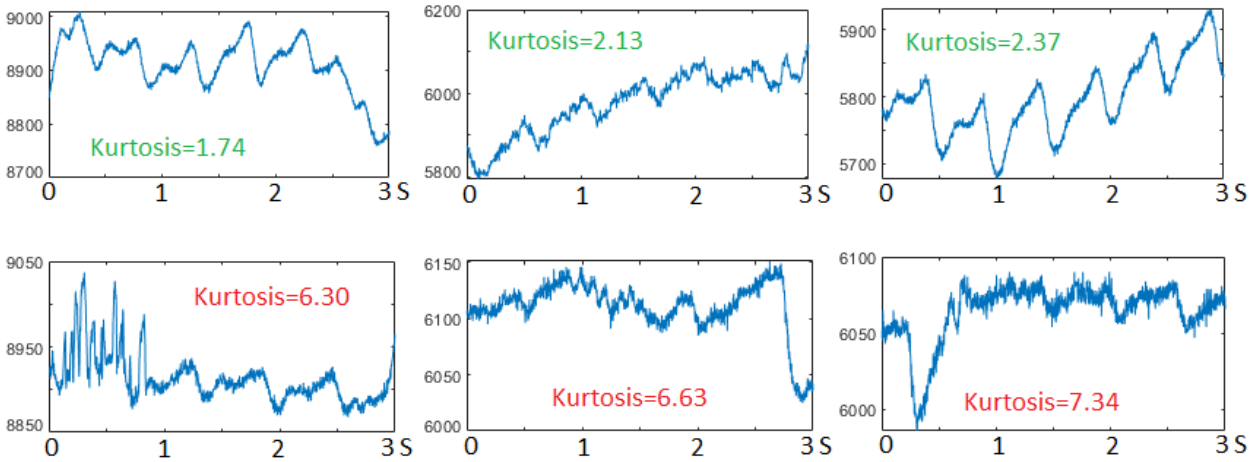

Figure 1. Example of 3-s length PPG trials

2.2. Feature Extraction

Recently, wavelet transform has been widely applied for extracting discriminative features from physiological signals by means of its wavelet type, translation, and scaling parameters (Prasad et al., 2021; Krishnan and Athavale, 2018). The wavelet transform is a convolution between the mother wavelet function $\psi_{m,n}(t)$ and the analyzed signal $f(t)$ in the time domain. It can be defined as follows

$$WTC\ (m,n) = n^{-1/2} \int f(t)\psi^{*}(\frac{t-m}{n})dt \qquad (2)$$

where *WTC* indicates the wavelet transform coefficients. Moreover, ψ*, *m* and *n* represent complex conjugate, translation, and scaling parameters, respectively. The multiplier factor of $n^{-1/2}$ normalizes the energy. Hence, it is taken into account as the same level for different values of *m* and *n*. The wavelet basis functions localize in time by *m* and capture the spatial frequency content by *n*, which provides the mother wavelet wider or narrower. In addition to the impact of scaling and translation parameters, the type of mother wavelet is a vital issue for the feature extraction phase. However, there is not a specified procedure for selecting the most suitable mother wavelet. Nevertheless, the previous applications or cross-validation

process can help to determine the useful mother wavelet (Aydemir, 2017). In this paper, we used the standard deviation and the average of *WTC*s as a feature, which was respectively calculated as follows:

$$S_{WTC} = \sqrt{\frac{1}{L-1}\sum (WTC - A_{WTC})^2} \tag{3}$$

$$A_{WTC} = \frac{1}{L}\sum WTC \tag{4}$$

where *L* represents the length of the *WTC*s.

2.3. Sequential Forward Mother Wavelet Selection Method

In this study, we used the SFMWS method (Aydemir et al., 2021), which selects a sufficient mother wavelet type combination on the training dataset. A general flowchart of the proposed method is given in Figure 2. In the training section, first, we independently extracted the features from the training dataset for each mother wavelet. Then, CAs were individually obtained for each mother wavelet and determined the most suitable single-use wavelet that achieved the highest leave-one-out cross-validation accuracy (LOOCVA). Afterward, the remaining mother wavelet's features were randomly added and re-evaluated to improve the previously obtained LOOCVA. This process was utilized until all considered mother wavelet combinations were assessed. It is worthwhile to mention that in every step for evaluating specific wavelet because the frequency band of the respiration is 0.04-1.6 Hz and the frequency band of the PPG signal pulse is in the range of 0.5-4 Hz. We searched for the best scale parameter of wavelet between 1.6 Hz and 4 Hz to avoid respiration artifact (Lee et al., 2007). After determining the most suitable mother wavelet(s) with their parameters, we applied the testing phase, which is illustrated with the green blocks in Figure 2. In this section, we predicted test trial labels and calculated the CA performance of the test set. The CA was calculated in terms of percentage as follows:

$$CA = \frac{NCPT}{TNT} x100 \tag{5}$$

where *NCPT* and *TNT* represent the number of correctly predicted trials and the total number of trials, respectively. We evaluated 13 different mother wavelets, including Symlet 2 (sym2), Symlet 3 (sym3),

Symlet 4 (sym4), Haar, Morlet (morl), Meyer (meyr), Mexican hat (mexh,) Coiflet 1 (coif1), Coiflet 2 (coif2), Coiflet 3 (coif3), Daubechies 1 (db1), Daubechies 2 (db2), and Daubechies 3 (db3). Since the wavelet transform was a time-consuming process, we proposed to use the *k*-NN classifier, which is a simple and fast algorithm (Timus and Bolat, 2017). The Euclidean distance metric was used to determine the most suitable *k* parameter of the classifier. It was searched between 1 and 15 with step size 1 in the training stage.

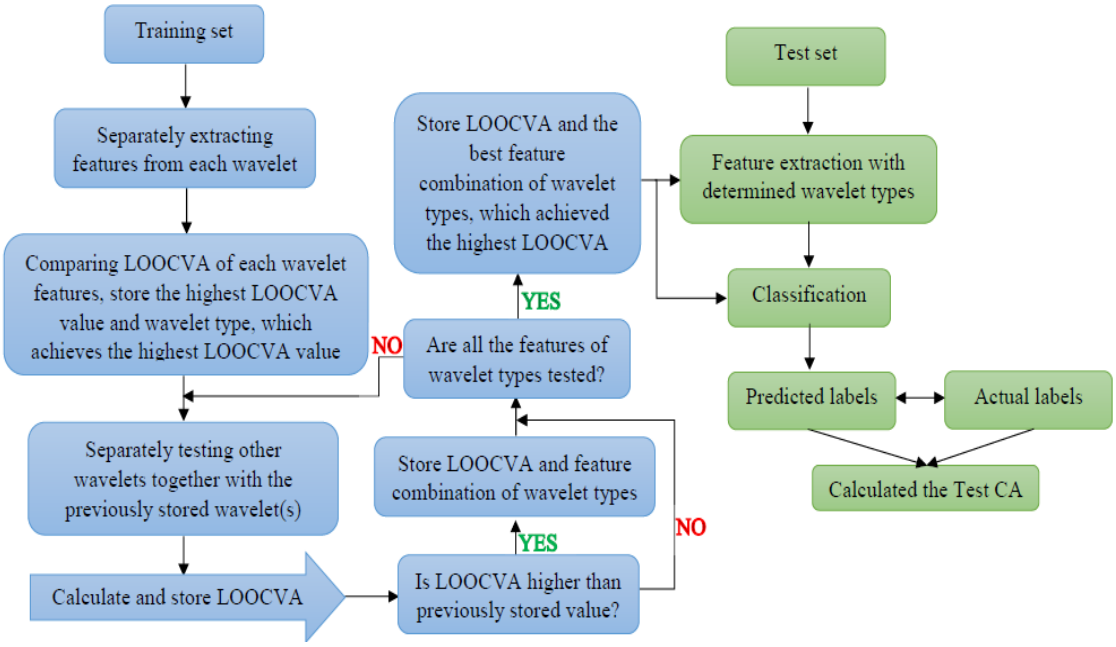

Figure 2. The flowchart of the SFMWS method

3. Results

In order to show the most suitable PPG length for PI, we tested the proposed method with different lengths of PPG trials, including 3 s, 4 s, 5 s, 6 s, and 7 s lengths. Moreover, the performance of the features, which were A_{WTC} and S_{WTC}, were individually calculated. The results are given in Table 2. In this table, the obtained mother wavelet combination and their intervals were given in parenthesis. As seen from the results, the highest performance was achieved as 88.64% with 7 s PPG lengths by sym4 mother wavelet. Contrary to this, the lowest CA was calculated by the combination of db2 and meyr as 63.27% with 4 s length trials. It should also be noted that morl and sym4 were the most frequently used mother wavelets, which were selected 6 and 5 times, respectively.

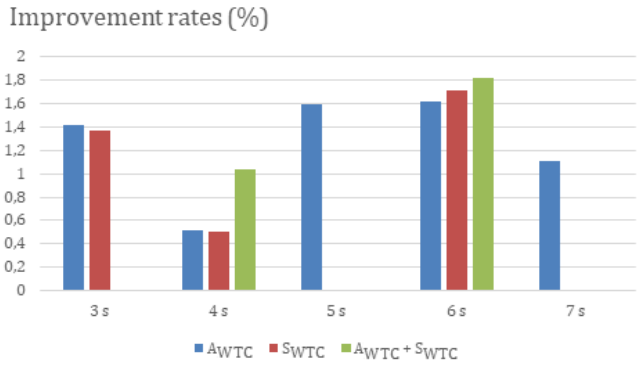

Figure 3. Improvement rates of the SFMWS method

Moreover, we calculated the CA improvement rates, which are given in Figure 2, by subtracting the CA of the first iteration from the last achieved CA performance. While the biggest improvement was provided for 6 s length trials with A_{WTC} + S_{WTC} features as 1.82%, there were no performance improvements for six different situations, where most of them were for A_{WTC} +S_{WTC} features. Figure 3 shows the improvement rates of SFMWS method. It should be noted that A_{WTC} provided improvements for 3s, 4s, 5s, 6s and 7s signals. However, S_{WTC} provided improvements only for the 3s, 4s and 6s signals. Moreover, their hybrid usage as A_{WTC} and S_{WTC} improved the CA rates only for 4s and 6s signals.

Table 2. The obtained results

Trial Length		**A_{WTC}**	**S_{WTC}**	**A_{WTC} + S_{WTC}**
3 s	Wavelet (scale)	morl (197-201) + haar (75-167) + meyr (87-171)	sym4 (143-171) + coif1 (71-95)	sym4 (71-79)
	CA	81.13	80.37	78.80
4 s	Wavelet (scale)	db2 (67-75) + meyr (71-119)	db2 (67-103) + sym4 (155-171)	morl (85-89) + db3 (71-95) + coif2 (71-75)
	CA	63.27	65.66	66.84
5 s	Wavelet (scale)	morl (81-105) + db2 (71-111)	morl (89-177)	Coif1 (85-97)
	CA	84.92	80.15	84.38
6 s	Wavelet (scale)	sym4 (115-179) + meyr (107-175)	meyr (153-157) + haar (79-175)	haar (168-248) +mexh (143-171)
	CA	78.86	76.92	83.64
7 s	Wavelet (scale)	morl (125-137) + mexh (71-75)	sym4 (159-175)	morl (93-101)
	CA	76.67	88.64	83.70

4. Conclusion

Parallel to the technological developments, the usage areas of biometric systems are getting more attention. Because of its properties like being safe and practically applicable, PPG-based biometry applications have attracted attention in recent years. In this paper, we proposed a kurtosis rejection-based PI method using PPG signals, which were recorded during a step exercise. Although the PPG signal-based PI studies were almost recorded during the resting state, we showed that PPG can be used for PI even it acquired during a step exercise. The highest CA was achieved with 7 s PPG segments as 88.64% by the *k*-NN classifier.

It is well-known that physical activities can significantly contaminate physiological signals. These undesired sources directly affect the performance of the machine learning applications. While the contamination level might be eliminated in some cases, the noise amplitude might be much higher than the physiological signals such that the trials could not be correctly classified. In this study, if the PPG trial has a kurtosis value greater than 5, we called it non-PPG and rejected it for classification. The results showed that the kurtosis rejection-based PI method increased the CA performance by 6.08% compared with the non-rejection process. Consequently, we believe that the proposed method can successfully identify subjects during a step exercise from their PPG signals.

Acknowledgment

The authors declare that there is no conflict of interest.

References

Alyasseri, Z. A. A., Khader, A. T., Al-Betar, M. A., & Alomari, O. A. (2020). Person identification using EEG channel selection with hybrid flower pollination algorithm. *Pattern Recognition*, 105, 107393.

Aydemir, O. (2020). Odor and Subject Identification Using Electroencephalography Reaction to Olfactory. *Traitement du Signal*, 37(5), 799-805.

Aydemir, O. (2017). Olfactory recognition based on EEG gamma-band activity. *Neural computation*, 29(6), 1667-1680.

Aydemir, T., Şahin, M., & Aydemir, O. (2021). Sequential Forward Mother Wavelet Selection Method for Mental Workload Assessment on N-back Task Using Photoplethysmography Signals. *Infrared Physics & Technology*, 103966.

Aydemir, T., Şahin, M., & Aydemir, O. (2020). A New Method for Activity Monitoring Using Photoplethysmography Signals Recorded by Wireless Sensor. *Journal of Medical and Biological Engineering*, 40(6), 934-942.

Bedagkar-Gala, A., & Shah, S. K. (2014). A survey of approaches and trends in person re-identification. *Image and vision computing*, 32(4), 270-286.

Biagetti, G., Crippa, P., Falaschetti, L., Saraceni, L., Tiranti, A., & Turchetti, C. (2020). Dataset from PPG wireless sensor for activity monitoring. *Data in brief*, 29, 105044.

Chao, X. U., Xiang, S. U. N., Ziliang, C. H. E. N., & Shoubiao, T. A. N. (2020). Exhaustive hard triplet mining loss for Person Re-Identification. *Turkish Journal of Electrical Engineering & Computer Sciences*, 28(5).

Choi, H. J., & Lee, J. Y. (2021). Comparative Study between Healthy Young and Elderly Subjects: Higher-Order Statistical Parameters as Indices of Vocal Aging and Sex. *Applied Sciences*, 11(15), 6966.

He, J., & Jiang, N. (2020). Biometric from surface electromyogram (sEMG): Feasibility of user verification and identification based on gesture recognition. *Frontiers in bioengineering and biotechnology*, 8, 58.

Jijomon, C. M., & Vinod, A. P. (2021). Person-identification using familiar-name auditory evoked potentials from frontal EEG electrodes. *Biomedical Signal Processing and Control*, 68, 102739.

Kavsaoğlu, A. R., Polat, K., & Bozkurt, M. R. (2014). A novel feature ranking algorithm for biometric recognition with PPG signals. *Computers in biology and medicine*, 49, 1-14.

Kim, G., Shu, D. W., & Kwon, J. (2021). Robust person re-identification via graph convolution networks. *Multimedia Tools and Applications*, 1-10.

Krishnan, S., & Athavale, Y. (2018). Trends in biomedical signal feature extraction. *Biomedical Signal Processing and Control*, 43, 41-63.

Lee, H. W., Lee, J. W., Jung, W. G., & Lee, G. K. (2007). The periodic moving average filter for removing motion artifacts from PPG signals. *International Journal of Control, Automation, and Systems*, 5(6), 701-706.

Li, Q., Dong, P., & Zheng, J. (2020a). Enhancing the security of pattern unlock with surface EMG-based biometrics. *Applied Sciences*, 10(2), 541.

Li, Y., Pang, Y., Wang, K., & Li, X. (2020b). Toward improving ECG biometric identification using cascaded convolutional neural networks. *Neurocomputing*, 391, 83-95.

Lu, L., Mao, J., Wang, W., Ding, G., & Zhang, Z. (2020). A study of personal recognition method based on EMG signal. *IEEE Transactions on Biomedical Circuits and Systems*, 14(4), 681-691.

Mazaira-Fernandez, L. M., Álvarez-Marquina, A., & Gómez-Vilda, P. (2015). Improving speaker recognition by biometric voice deconstruction. *Frontiers in bioengineering and biotechnology*, 3, 126.

Pinto, J. R., Cardoso, J. S., Lourenço, A., & Carreiras, C. (2017). Towards a continuous biometric system based on ECG signals acquired on the steering wheel. *Sensors*, 17(10), 2228.

Prasad, D. S., Chanamallu, S. R., & Prasad, K. S. (2021). Mitigation of ocular artifacts for EEG signal using improved earth worm optimization-based neural network and lifting wavelet transform. *Computer Methods in Biomechanics and Biomedical Engineering*, 24(5), 551-578.

Rodrigues, D., Silva, G. F., Papa, J. P., Marana, A. N., & Yang, X. S. (2016). EEG-based person identification through binary flower pollination algorithm. *Expert Systems with Applications*, 62, 81-90.

Siam, A. I., Abou Elazm, A., El-Bahnasawy, N. A., El Banby, G. M., & Abd El-Samie, F. E. (2021). PPG-based human identification using Mel-frequency cepstral coefficients and neural networks. *Multimedia Tools and Applications*, 1-19.

Timus, O. H., & Bolat, E. D. (2017). k-NN-based classification of sleep apnea types using ECG. *Turkish Journal of Electrical Engineering & Computer Sciences*, 25(4), 3008-3023.

Xiao, J., Hu, F., Shao, Q., & Li, S. (2019). A low-complexity compressed sensing reconstruction method for heart signal biometric recognition. *Sensors*, 19(23), 5330.

Wilaiprasitporn, T., Ditthapron, A., Matchaparn, K., Tongbuasirilai, T., et.al., (2019). Affective EEG-

based person identification using the deep learning approach. *IEEE Transactions on Cognitive and Developmental Systems*, 12(3), 486-496.

Wu, S. C., Chen, P. T., Swindlehurst, A. L., & Hung, P. L. (2018). Cancelable biometric recognition with ECGs: subspace-based approaches. *IEEE Transactions on Information Forensics and Security*, 14(5), 1323-1336.

Zhang, X., & Ding, Q. (2016). Respiratory rate monitoring from the photoplethysmogram via sparse signal reconstruction. *Physiological measurement*, 37(7), 1105.